Applied Physics Letters ARTICLE pubs.aip.org/aip/apl

Defect evolution in proton-irradiated 4H-SiC

Cite as: Appl. Phys. Lett. **127**, 202101 (2025); doi: 10.1063/5.0289493
Submitted: 8 July 2025 · Accepted: 2 November 2025 ·
Published Online: 17 November 2025

Huifan Xiong,[1,2] Shuai Liu,[2] Lihui Song,[1,2,a)] Deren Yang,[1,2] and Xiaodong Pi[1,2,3,a)]

AFFILIATIONS

[1]State Key Laboratory of Silicon and Advanced Semiconductor Materials and School of Materials Science and Engineering, Zhejiang University, Hangzhou 310027, China
[2]Key Laboratory of Power Semiconductor Materials and Devices of Zhejiang Province and Institute of Advanced Semiconductors, ZJU-Hangzhou Global Scientific and Technological Innovation Center, Zhejiang University, Hangzhou 311200, China
[3]Shangyu Institute of Semiconductor Materials, Zhejiang University, Shaoxing 212399, China

[a)]**Authors to whom correspondence should be addressed:** songlihui@zju.edu.cn and xdpi@zju.edu.cn

ABSTRACT

4H silicon carbide (4H-SiC) is a critical material for power electronics used in extreme radiation environments such as spacecraft and nuclear reactors. Among all kinds of radiations, proton radiation needs to be well investigated since defects induced by proton irradiation seriously impact device reliability. Crucially, this work uniquely investigates the impact of irradiation direction and energy by exposing 4H-SiC Schottky barrier diodes (SBDs) to proton radiation at five distinct energies with the same dose from both the front and back sides to systematically study energy-and-direction dependent defect formation. Combining high-sensitivity deep-level transient spectroscopy (DLTS) with Monte Carlo-based SRIM simulations, we achieve precise spatial correlation between experimental calculated defect profiles and theoretical displacement damage models. It is found that lower-energy protons tend to generate a higher density of defects in the depletion region. Notably, backside irradiation with 8.5 MeV protons results in a significantly larger defect concentration within the depletion region compared to front-side irradiation with the same energy, highlighting the directional sensitivity of irradiation-induced defects. Finally, the effects of both low-temperature and high-temperature annealing on radiation-induced defects are investigated.

Silicon carbide (SiC), a prominent wide-bandgap semiconductor, exhibits exceptional physical properties, including high electron saturation velocity and high breakdown field.[1–5] Its inherent radiation resistance and high thermal conductivity render it exceptionally well-suited for prolonged operation in harsh environments, such as aerospace and nuclear energy sectors.[6–9] However, prolonged proton irradiation poses challenges, where cumulative displacement damage compromises device performance and reliability.[10–13] Displacement damage is a significant irradiation effect, characterized by its long-term stability in materials and its cumulative impact with increasing irradiation dose.[14,15] Among the various forms of displacement damage, electro-active point defects introduced during irradiation have a more substantial impact on device performance.[16,17]

Several techniques can detect irradiation-induced defects, including photoluminescence spectroscopy (PL), electron paramagnetic resonance (EPR), and deep-level transient spectroscopy (DLTS). Nevertheless, PL is limited to identifying defects associated with radiative recombination, while EPR can only detect defects with unpaired electrons.[18–20] DLTS detects electro-active defects and can theoretically identify defects down to a concentration of $1 \times 10^9\,\mathrm{cm}^{-3}$. DLTS can determine the charge transition levels (CTLs) of the defects in SiC, which manifest as peaks in DLTS spectra. For instance, the $Z_{1/2}$ defect was regarded as V_C that occurs at approximately E_C-0.63 eV for the (2-/0) levels, while the $EH_{6/7}$ defects occur at around E_C-1.5 eV for the (0/+) levels.[21–23] The $Z_{1/2}$ defect has been proved to be the non-radiative recombination center and a significant lifetime killer.[24,25] The S_1(E_C-0.4 eV) and S_2 (E_C-0.71 eV) peaks correspond to the CTLs of V_{Si} (3-/2-) and V_{Si} (2-/-), respectively.[26,27] The EH_4 (E_C-0.91 eV) defect has been regarded to the carbon antisite-carbon vacancy pairs ($C_{Si}V_C$), whereas the attribution of the EH_5 (E_C-1.15 eV) defect remains controversial.[28,29]

Irradiation studies on SiC, in the literature, have predominantly focused on particle type, dose, and temperature. Nevertheless, the influence of irradiation direction on SiC material and device properties, crucial for altering defect spatial distribution and density, remains largely unexplored. In this study, we investigate the defects introduced into the depletion region of SiC by protons with varying energies and irradiation directions. We utilized the Stopping and Range of Ions in Matter (SRIM) simulation to determine the projected range of protons in SiC at different energies. For instance, 240 KeV and 8.5 MeV

protons have projected ranges that approximately reach the depth of the depletion region under the default reverse voltage in DLTS and the thickness of the SiC sample, respectively. Consequently, we selected protons with five representative energies of 240 KeV, 3 MeV, 8.5, 30, and 50 MeV to irradiate the SiC Schottky barrier device in order to examine the effect of proton energy on defect formation. Notably, the selected energy ranges represent common proton energies in space and hold significant research value.[30–32] Additionally, a front/back irradiation comparison was conducted to examine the influence of irradiation direction on depletion region defect formation. We employed DLTS with a low detection limit to characterize the defects in the irradiated SiC. Then the identities and electrical parameters of the defects introduced under different irradiation conditions were compared. Last, we investigated the thermal stability of the irradiation-induced defects via annealing the irradiated samples at various temperatures.

The 13 μm thick n-doped (5×10^{15} cm^{-3}) 4H silicon carbide (4H-SiC) epilayers were prepared by chemical vapor deposition (CVD) upon 4H-SiC substrates. After RCA cleaning, a 200 nm thick layer of nickel (Ni) was deposited on the C-face of the SiC, followed by annealing at 1273 K for one minute under flowing nitrogen gas in a rapid thermal processing furnace (RTP) to form Ohmic contact. Next, Ni was deposited on the Si-face of the SiC using a mask with 1 mm diameter holes, followed by 773 K annealing for 2 min to form Schottky contact. The prepared SiC Schottky barrier diodes (SBDs) were subjected to proton irradiation at a constant dose of 5×10^{12} cm^{-2} but with varying energies of 0.24, 3, 8.5, 30, and 50 MeV. We also performed back proton irradiation at these energies. A schematic representation of the proton irradiation applied to the SiC SBDs is shown in Fig. 1(a).

DLTS can detect defects in the space charge region, which play a critical role in device performance. It extracts defect information from transient capacitance changes induced by a periodic voltage. Initially, the metal–semiconductor (MS) junction is reverse-biased [see Fig. 1(b)], resulting in many empty traps. When a pulse voltage is applied, the energy bands recover, and electrons begin to fill the empty traps below the Fermi energy level as shown in Fig. 1(c). Upon reverting to reverse bias, trapped electrons emit back into the conduction band and induce capacitance changes, as illustrated in Fig. 1(d). The radiation-induced defects were characterized using the DLTS tool DLS-80D, produced by SEMILAB, operating in lock-in capacitance mode. DLTS spectra were recorded over a temperature range of 100–800 K, with the cooling control system based on the volatilization of liquid nitrogen in a Dewar cryostat. DLTS measurements conducted temperature scans in a vacuum sample chamber at a heating rate of 0.2 K/s. Once the target temperature was reached, it was maintained for 4 min. The parameters used for DLTS measurements were as follows: a filling pulse voltage of $V_p = 0$ V, a pulse width of $t_p = 42$ μs, and a reverse bias of $V_r = -5$ V.[12,33] The 42 μs pulse width is sufficient for electrons to fully fill the empty traps.

DLTS spectra, shown in Fig. 2, indicate that the types of defects introduced by various irradiation conditions are consistent. To ascertain the defect identities, multi-frequency temperature scans were performed [Fig. 2(c)], and then the energy levels of the respective defect peaks were calculated through Arrhenius plot fitting [Fig. 2(d)]. Proton irradiation predominantly introduces the $Z_{1/2}$ (E_C-0.66 eV) defect, which is considered a carbon vacancy, accompanied by S_1 and S_2 defects. The S_1 (E_C-0.38 eV) and S_2 (E_C-0.74 eV) defects are identified as silicon vacancies.[26,27] Table I shows the concentration of various

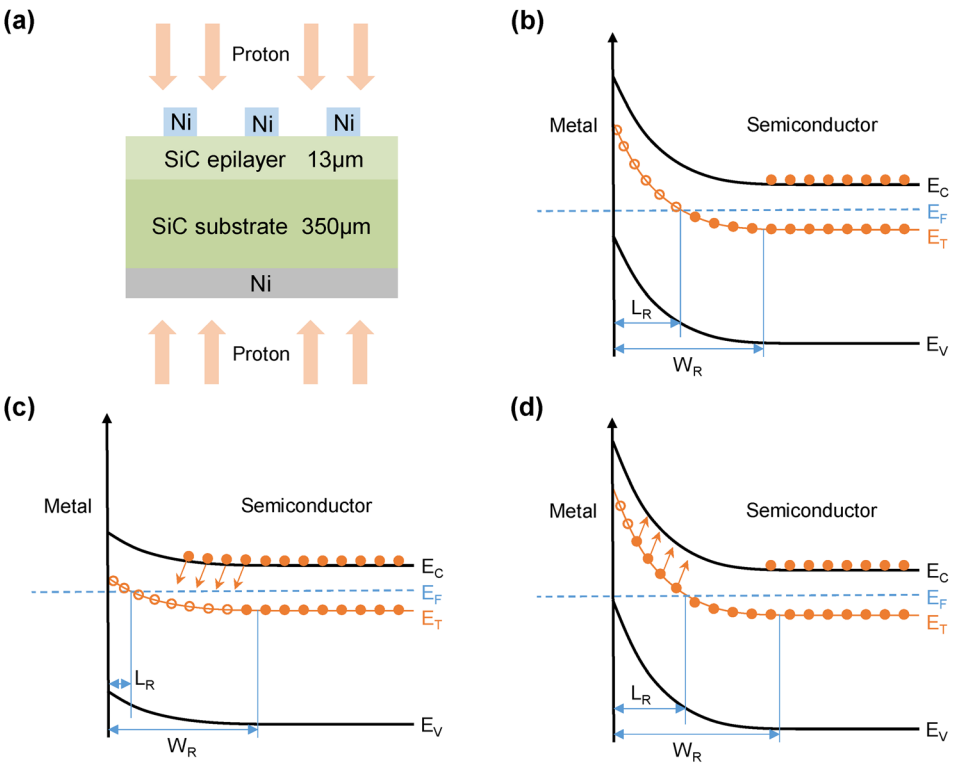

FIG. 1. Experimental setup and DLTS principle. (a) Schematic diagram illustrating the proton irradiation processes for a 4H-SiC Schottky Barrier Diode (SBD). Energy band diagrams of the metal–semiconductor junction (b) before the filling pulse, (c) during the filling pulse, and (d) just after the filling pulse.

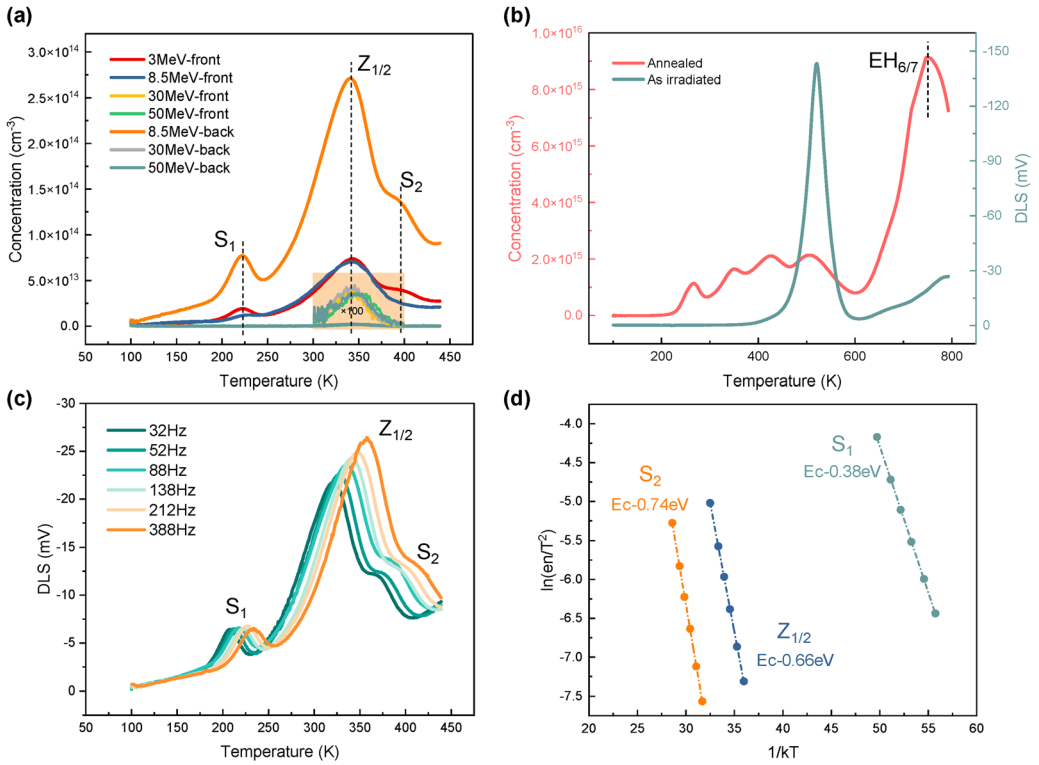

FIG. 2. DLTS measurements of 4H-SiC SBDs under different proton irradiation conditions. (a) The DLTS concentration spectrum of SiC irradiated under various conditions after annealing at 480 K. To eliminate the effects of instability defects, the samples were annealed at 480 K before testing. (b) The DLTS spectrum of SiC irradiated with 240 KeV protons before (green line) and after (yellow line) annealing at 1173 K. (c) DLTS spectra measured at different frequencies and (d) the Arrhenius fitting.

defects introduced in SiC by proton irradiation under different conditions at a constant dose of $5 \times 10^{12}\,\mathrm{cm}^{-2}$. It can be seen from Table I that 8.5 MeV backside proton irradiation introduces a higher concentration of defects in the SiC epilayer than front-side irradiation, demonstrating the significance of irradiation direction. Furthermore, it is found that irradiation with 30 and 50 MeV protons introduces negligible point defects within the SiC depletion regions compared to low-energy proton irradiation, while 240 KeV proton irradiation introduces a substantial number of point defects within the depletion region, as illustrated in Fig. 2(b). In these conditions, the compensation effect, as a result of the high concentrations of irradiation-induced deep-level defects trapping the electrons, occurs, which is able to shift the Fermi level of SiC to the middle of the bandgap. Please note that when the Fermi level shifts below the energy level of the detecting defects, applying either a filling voltage or a reverse bias voltage can no longer induce a DLTS signal, as no electron emission from the defects can occur in this case. Therefore, low-energy-level defects cannot be detected by DLTS, which appears as an absence of defect peaks in the low-temperature region of the DLTS spectra. Basically, this phenomenon of the DLTS spectrum is able to reveal the position of the Fermi level,

TABLE I. The concentrations of $Z_{1/2}$, S_1, and S_2 defects induced by proton irradiation in different conditions. The slash denotes no detected DLTS signal. The slash in the table indicates that the defect was not detected by the DLTS equipment.

Proton energy (MeV)	Direction	$Z_{1/2}$ concentration (cm^{-3})	S_1 concentration (cm^{-3})	S_2 concentration (cm^{-3})
0.24	Front	9.13×10^{15}	⋯	⋯
3	Front	7.03×10^{13}	1.91×10^{13}	2.35×10^{13}
8.5	Front	7.39×10^{13}	1.18×10^{13}	1.48×10^{13}
	Back	2.72×10^{14}	7.72×10^{13}	8.41×10^{13}
30	Front	2.16×10^{12}	⋯	⋯
	Back	2.47×10^{12}	⋯	⋯
50	Front	2.06×10^{12}	⋯	⋯
	Back	1.96×10^{12}	⋯	⋯

TABLE II. The projection ranges of proton irradiation with various energies in SiC.

Proton energy (MeV)	Projection range (μm)	Longitudinal straggling (μm)	Lateral straggling (μm)
0.24	1.47	0.09	0.13
3	61.46	2.66	2.73
8.5	363.67	15.77	14.61
30	3390	145.78	125.35
50	8450	365.51	303.81

which lies slightly above the energy level of the lowest-energy level of the detectable defect. Nevertheless, these defects can again be partially detected after high-temperature (1173 K) annealing, which is able to eliminate metastable defects and thus attenuates the compensation effect leading to the upward shift of the Fermi level.

To further analyze the influence of irradiation energy and direction on defect introduction, SRIM simulations were employed to determine the projection range of protons of varying energies in SiC (Table II). Table II indicates that the penetration depth of protons increases with increasing proton energy. During proton irradiation of SiC, the energy loss rate exhibits a Bragg peak at the end of the projection range, resulting in a peak of vacancy concentration in this region. Figure 3 presents the depth profiles of carbon vacancy concentrations introduced by proton irradiation at different energies in SiC. The projection range of 8.5 MeV protons in SiC approximately equals the sample thickness, thus backside irradiation introduces a high concentration of defects in the epilayer. To compare defect concentrations induced by different irradiation conditions, carbon vacancy concentration was chosen as a reference, and DLTS-measured carbon vacancy concentrations were compared with SRIM-simulated carbon vacancy concentrations. In the DLTS spectra, the ratio of $Z_{1/2}$ concentration to $EH_{6/7}$ concentration is 2:1, and thus, half of the $Z_{1/2}$ concentration is regarded as the carbon vacancy concentration.[34,35] To eliminate the influence of stress and other important factors on carbon vacancy concentration, the irradiated samples were annealed at 480 K for 5 min.[12] A summary of carbon vacancy concentration introduced into SiC under different irradiation conditions is shown in Fig. 3(f). The trends of the experimental and simulation results are consistent, although the experimental results demonstrate slightly lower carbon vacancy concentration. It is important to note that SRIM simulations, by assuming all ion collisions produce vacancies and neglecting temperature effects, ignore key processes in real materials such as defect recombination, migration, and annihilation. The discrepancy between simulation and experimental results can be explained by the theory below: room-temperature irradiation conditions allow for the recombination of Frenkel pairs consisting of vacancies and the nearby radiation-induced interstitials.[36] Silicon vacancy–silicon interstitial Frenkel pairs in SiC require a recombination energy barrier of less than ~0.2 eV, whereas carbon interstitial–carbon vacancy pairs require an energy barrier of 0.4 eV.[37] Moreover, defect annealing in SiC can proceed with an energy barrier as low as 0.25 eV, enabling recombination at 220 K with a sizable rate,[38] which supports that nearby interstitials and vacancies

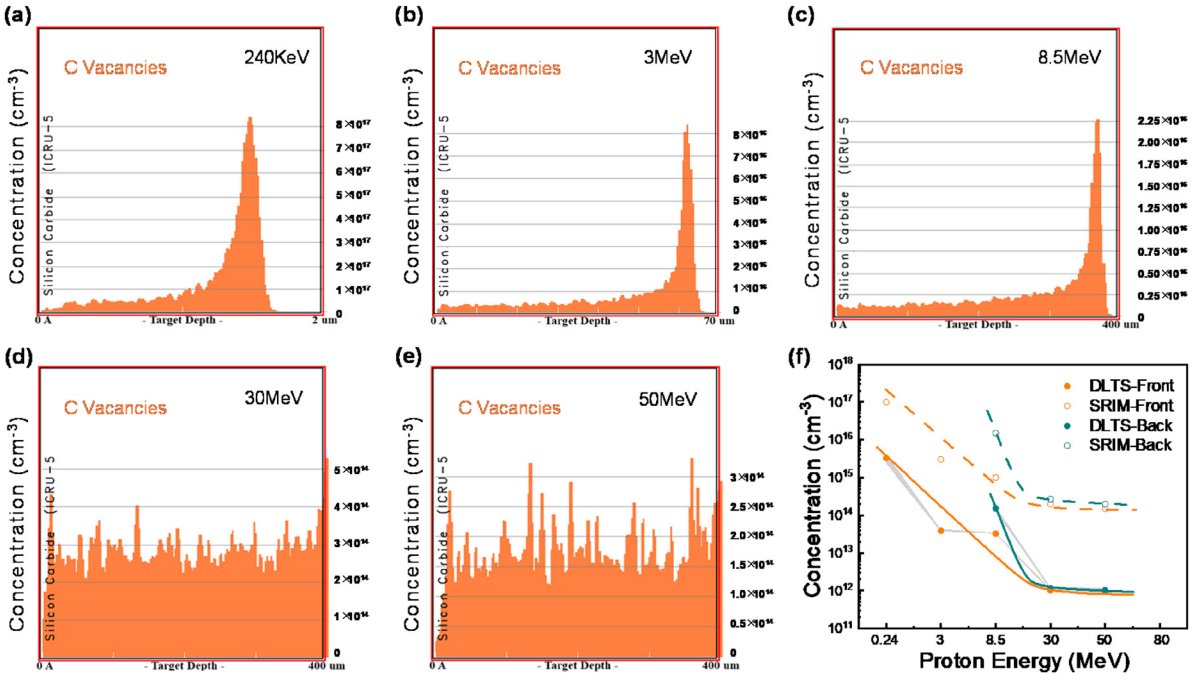

FIG. 3. The concentration of carbon vacancies induced by proton irradiation in different energies simulated via SRIM and measured via DLTS. The carbon vacancy concentration vs projection depth simulated by SRIM after proton irradiation in energies of (a) 240 KeV, (b) 3 MeV, (c) 8.5 MeV, (d) 30 MeV, and (e) 50 MeV. (f) A comparative analysis of DLTS calculated carbon vacancy concentration and SRIM-simulated carbon vacancy concentration illustrating the variation of carbon vacancy concentration with different irradiation energies and directions.

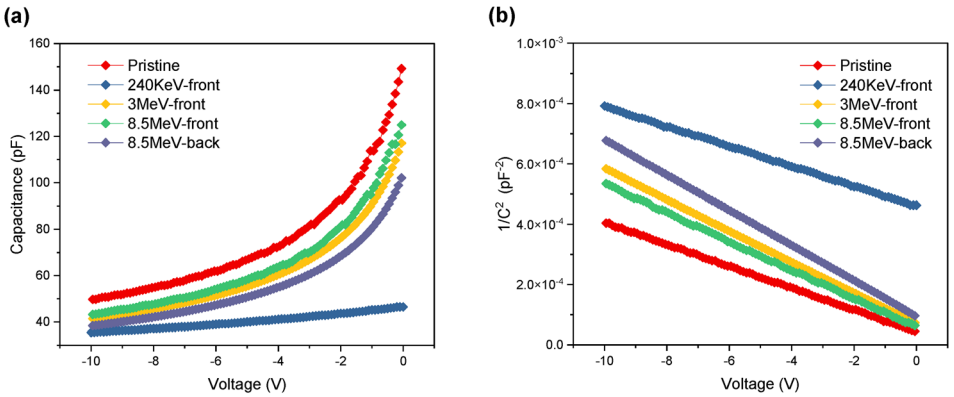

FIG. 4. The C–V measurement results of 4H-SiC SBDs before and after proton irradiation. (a) Capacitance and (b) $1/C^2$ vs voltage characteristics of the SBDs irradiated with protons in different conditions.

in SiC can undergo recombination at room temperature with a substantial rate. Overall, displacement damage in SiC devices is more pronounced under two conditions: low-energy proton irradiation and high-energy proton irradiation from the backside.

Figure 4 illustrates the impact of varying irradiation conditions on the electrical parameter (capacitance) of the SBD devices. It is found that irradiation-induced defects lead to a reduction in capacitance. Furthermore, 8.5 MeV proton irradiation from the backside exhibits a more pronounced effect on capacitance decline compared to front-side irradiation. Moreover, for front-side irradiation, lower-energy protons induce a greater reduction in the SBD device's capacitance. These observations are consistent with the results obtained from DLTS as illustrated above. The effective carrier concentrations and barrier heights can further be extracted by fitting the slope of the $1/C^2$–V curves, as shown in Table III. The increase in irradiation-induced defect density is found to result in a lower effective carrier concentration and a higher Schottky barrier height. This is primarily attributed to the introduction of acceptor-like defects that can compensate electrons. The changes in effective carrier concentrations and Schottky barrier heights are exacerbated by the increasing compensation effect. Whereas, for samples irradiated with 240 KeV protons, the shallow damage profile and the resulting high compensation effect caused by high concentrations of surface defects cause the C–V curves to flatten,[4,12,39] exhibiting reduced voltage dependence. Consequently, the fitting procedure for calculating carrier concentration and barrier height becomes unreliable. In summary, both the proton energy and the irradiation direction play a critical role in determining the extent and distribution of radiation-induced defects. The defect concentration peak at the end of the projection range, which is influenced by proton energy and direction, demonstrates new insights for radiation protection.

Interestingly, when comparing electron irradiation with proton irradiation after annealing at different temperatures (See Fig. 5), we

TABLE III. The carrier concentrations and barrier heights extracted from the $1/C^2$–V curve fitting in Fig. 4. The slash in the table indicates that C–V fitting is no longer applicable due to high compensation effects.

Irradiation condition	Pristine	240 KeV-front	3 MeV-front	8.5 MeV-front	8.5 MeV-back
Carrier concentration ($\times 10^{15}$ cm^{-3})	5.0	···	3.52	3.81	3.10
Barrier height (eV)	1.42	···	1.58	1.46	1.89

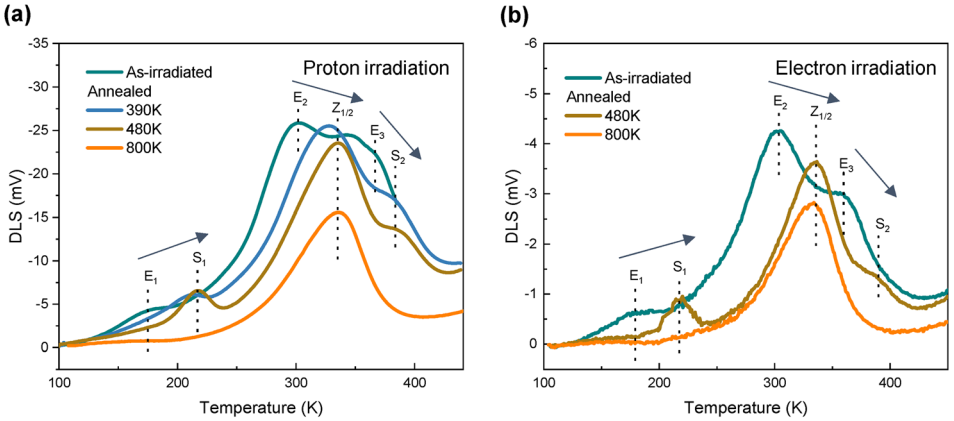

FIG. 5. Transformations in DLTS peak when subjected to annealing. (a) DLTS spectra of the proton-irradiated SiC before and after annealing at temperatures of 390, 480, and 800 K. (b) DLTS spectra of the electron-irradiated SiC before and after annealing at temperatures of 480 and 800 K.

observed DLTS peaks shifted in both cases. In the DLTS spectrum, three unstable defect peaks shifted to higher temperatures in the 390–440 K range, corresponding to transitions from E_1 to S_1, E_2 to $Z_{1/2}$, and E_3 to S_2. These defects have been reported in SiC irradiated with various charged particles, including protons and electrons.[12,40,41] This transformation phenomenon is inferred to result from the reduction of defect clusters after annealing. Initially, the energy levels of the defects were altered by the stress from the surrounding defect clusters induced by irradiation, leading to changes in the DLTS spectrum. After the defect clusters are annealed out at temperatures above 390 K, the energy levels of the above defects return to normal value, and so does the DLTS spectrum. Additionally, when the annealing temperature is further increased, we observe that the S_1 and S_2 defects are annealed out at 800 K. Comparing the DLTS spectra of SiC irradiated by protons and electrons, we find that the types of defects induced by proton and electron irradiation are the same. However, electron irradiation provides more thermal energy, due to the ionizing effect, to the samples compared to proton irradiation. As a result, the concentration of the defects induced by the two irradiation methods is slightly different, influenced by both the electron dose and the cooling method.

To explore the thermal stability of the remaining stable defects, we annealed the SiC samples irradiated with 8.5 MeV protons at various higher temperatures for 20 min and then measured the DLTS spectrum (Fig. 6). The $Z_{1/2}$ and $EH_{6/7}$ defects, known as carbon vacancies, can stably exist at 1523 K, consistent with the reported literature.[42] The EH_4 and EH_5 defects were previously considered as the (+/0) level of $C_{Si}V_C$ with different configurations.[43] However, the identification of the EH_5 defect has recently been questioned.[22,29] As shown in Fig. 4, the EH_5 defect annealed out at 873 K, while the EH_4 defect annealed out at 1473 K. Therefore, EH_4 and EH_5 defects should not both be attributed to the $C_{Si}V_C$ defect, given that different $C_{Si}V_C$ configurations exhibit nearly identical formation energy.[43–45] Moreover, the EH_5 defect can be generated by low-energy electrons, which primarily displace carbon atoms and generate carbon-related defects,[29,46] which also indicate that they are different types of defects. Therefore, the EH_5 defect is a metastable defect related only to a carbon atom or carbon vacancy instead of the $C_{Si}V_C$ defect.

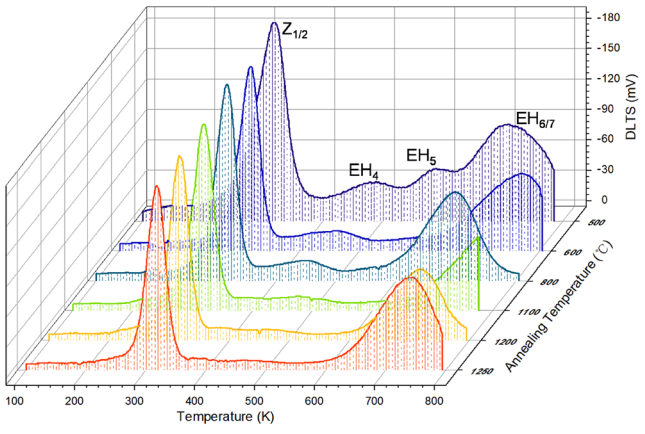

FIG. 6. Thermal stability of the common irradiation-induced defects in SiC. DLTS spectra of the common irradiation-induced defects in SiC after annealing at temperatures of 773, 873, 1073, 1373, 1473, and 1523 K following proton irradiation.[2]

The irradiation-induced defect evolution in SiC was studied after proton irradiation with different energies and incident directions and subsequent annealing. The results demonstrate that lower-energy protons generate a higher number of defects within the depletion region due to the short projection range and less ionizing effect, which significantly deteriorates device performance. Furthermore, 8.5 MeV protons generate more defects within the depletion region during backside radiation compared to front-side radiation, as the highest defect concentration occurs at the end of the proton projection path. The simulation results show a good alignment with the experimental findings, confirming the validity of the above theory. Consequently, it emphasizes the importance of implementing radiation shielding at the back of the SiC device during packaging for radiation hardening. In addition, the thermal energy introduced during the proton irradiation is able to partially anneal out some unstable defects and stress. Last, this study investigated the thermal stability of some common irradiation-induced defects in SiC, finding the priority of thermal stability of these irradiation-induced defects and an evidence that the EH_4 and EH_5 defects are not the same type of defect as reported in previous literature.

This work was supported by the Zhejiang Provincial Natural Science Foundation (Grant No. LMS25F040003), the Open Fund of the Key Laboratory of Power Semiconductor Materials and Devices of Zhejiang Province (Grant No. 2022E10015), and the Program of Qianjiang Distinguished Experts of Hangzhou.

AUTHOR DECLARATIONS

Conflict of Interest

The authors have no conflicts to disclose.

Author Contributions

Huifan Xiong: Investigation (equal); Software (equal); Validation (equal); Visualization (equal); Writing – original draft (equal); Writing – review & editing (equal). **Shuai Liu:** Investigation (equal); Methodology (equal); Validation (equal). **Lihui Song:** Funding acquisition (equal); Investigation (equal); Methodology (equal); Project administration (equal); Resources (equal); Supervision (equal); Validation (equal); Writing – review & editing (equal). **Deren Yang:** Conceptualization (equal); Formal analysis (equal); Methodology (equal); Project administration (equal); Supervision (equal). **Xiaodong Pi:** Funding acquisition (equal); Investigation (equal); Methodology (equal); Project administration (equal); Supervision (equal); Writing – review & editing (equal).

DATA AVAILABILITY

The data that support the findings of this study are available from the corresponding author upon reasonable request.

REFERENCES

[1]X. Chen, X. Yang, X. Xie, Y. Peng, L. Xiao, C. Shao, H. Li, X. Hu, and X. Xu, "Research progress of large size SiC single crystal materials and devices," Light. Sci. Appl. **12**(1), 1037 (2023).

[2]K. Yamaguchi, D. Kobayashi, T. Yamamoto, and K. Hirose, "Theoretical investigation of the breakdown electric field of SiC polymorphs," Phys. B **532**, 99 (2018).

[3]A. Arvanitopoulos, M. Antoniou, S. Perkins, M. Jennings, M. Belanche, K. Gyftakis, and N. Lophitis, "On the suitability of 3C-silicon carbide as an alternative to 4H-silicon carbide for power diodes," IEEE Trans. Ind. Appl. **55**(4), 4080 (2019).
[4]J. M. Rafí, G. Pellegrini, P. Godignon, S. O. Ugobono, G. Rius, I. Tsunoda, M. Yoneoka, K. Takakura, G. Kramberger, and M. Moll, "Electron, neutron, and proton irradiation effects on SiC radiation detectors," IEEE Trans. Nucl. Sci. **67**, 12 (2020).
[5]G. Yang, L. Xu, C. Cui, X. Pi, D. Yang, and R. Wang, "Anisotropic etching mechanisms of 4H-SiC: Experimental and first-principles insights," J. Semicond. **45**, 012502 (2024).
[6]Y. Wang, J. C. Zhou, M. Lin, X. J. Li, J. Q. Yang, and F. Cao, "A comparative study of single-event-burnout for 4H-SiC UMOSFET," IEEE J. Electron Devices Soc. **10**, 373 (2022).
[7]T. Zhenyu, T. Xiaoyan, Z. Yimeng, Z. Pu, S. Yuyin, and Z. Yuming, "4H-SiC integrated circuits for high-temperature applications," J. Cryst. Growth **605**, 127060 (2023).
[8]M. B. Li, F. Cao, H. F. Hu, X. J. Li, J. Q. Yang, and Y. Wang, "High single-event burnout resistance 4H-SiC junction barrier Schottky diode," IEEE J. Electron Devices Soc. **9**, 591 (2021).
[9]Y. Pei, W. Geng, L. Xu, C. Cui, X. Pi, D. Yang, and R. Wang, "Demonstration of irradiation-resistant 4H-SiC based photoelectrochemical water splitting," J. Semicond. **45**, 112503 (2024).
[10]L. Mo, Q. Yu, Z. Hu, B. Zhou, T. Yi, L. Yuan, L. Lin, F. Shen, and T. Liang, "Single event burnout of SiC MOSFET induced by atmospheric neutrons," Microelectron. Reliab. **146**, 114997 (2023).
[11]Y. Sun, X. Wan, Z. Liu, J. Hu, J. Yan, X. Li, and Y. Shi, "Investigation of total ionizing dose effects in 4H-SiC power MOSFET under gamma ray radiation," Radiat. Phys. Chem. **197**, 110219 (2022).
[12]H. Xiong, X. Lu, X. Gao, Y. Yan, S. Liu, L. Song, D. Yang, and X. Pi, "Defects evolution in n-type 4H-SiC induced by electron irradiation and annealing," J. Semicond. **45**, 072502 (2024).
[13]Y. Li, X. Gao, J. Gao, Z. Yang, M. Gong, M. Huang, Y. Ma, and T. Yu, "Influence of annealing treatment on performance of 4H-SiC SBD irradiated by heavy ions under room temperature and low temperature," Micro Nanostruct. **194**, 207945 (2024).
[14]L. Wu, S. Dong, F. Liu, Z. Liu, Y. Wei, W. Li, X. Xu, J. Yang, and X. Li, "Analysis of displacement damage induced by silicon-ion irradiation in SiC MOSFETs," IEEE Trans. Nucl. Sci. **71**(7), 1370 (2024).
[15]S. Bonaldo, C. Martinella, S. Race, N. Für, S. Mattiazzo, M. Bagatin, S. Gerardin, A. Paccagnella, and U. Grossner, "Radiation-induced effects in SiC vertical power MOSFETs irradiated at ultrahigh doses," IEEE Trans. Nucl. Sci. **71**(4), 418 (2024).
[16]C. S. Tan, "Electrical conductivity improvement of point defects in 4H-SiC," Cryst. Growth Des. **23**, 6250 (2023).
[17]E. Omotoso, A. T. Paradzah, P. J. Janse van Rensburg, M. J. Legodi, F. D. Auret, E. Igumbor, H. T. Danga, M. Diale, and W. E. Meyer, "Electrical characterisation of deep level defects created by bombarding the n-type 4H-SiC with 1.8 MeV protons," Surf. Coat. Technol. **355**, 2 (2018).
[18]M. E. Zvanut, "Electron paramagnetic resonance characterization of SiC," in *SiC Power Materials: Devices and Applications* (Springer Berlin Heidelberg, Berlin, Heidelberg, 2004).
[19]C. Kawahara, J. Suda, and T. Kimoto, "Identification of dislocations in 4H-SiC epitaxial layers and substrates using photoluminescence imaging," Japanese J. Appl. Phys. **53**(2), 020304 (2014).
[20]S. P. Pavunny, A. L. Yeats, H. B. Banks, E. Bielejec, R. L. Myers-Ward, M. T. DeJarld, A. S. Bracker, D. K. Gaskill, and S. G. Carter, "Arrays of Si vacancies in 4H-SiC produced by focused Li ion beam implantation," Sci. Rep. **11**(1), 82832 (2021).
[21]J. Park, B.-G. Park, H. Baek, and G.-M. Sun, "Electrical characteristics and deep-level transient spectroscopy of a fast-neutron-irradiated 4H-SiC Schottky barrier diode," Nucl. Eng. Technol. **55**(1), 201 (2023).
[22]C. Hemmingsson, N. T. Son, O. Kordina, J. P. Bergman, E. Janzén, J. L. Lindström, S. Savage, and N. Nordell, "Deep level defects in electron-irradiated 4H SiC epitaxial layers," J. Appl. Phys. **81**(9), 6155 (1997).
[23]T. Lin, S. H. Li, L. P. Ho, A. Kuznetsov, H. N. Lee, T. Chau, and F. C. C. Ling, "Suppression of the carbon vacancy traps and the corresponding leakage current reduction in 4H-SiC diodes by low-temperature implant activation in combination with oxidation," IEEE Electron Device Lett. **44**(4), 578 (2023).
[24]T. Kimoto, H. Niwa, T. Okuda, E. Saito, Y. Zhao, S. Asada, and J. Suda, "Carrier lifetime and breakdown phenomena in SiC power device material," J. Phys. D:Appl. Phys. **51**, 363001 (2018).
[25]L. Storasta and H. Tsuchida, "Reduction of traps and improvement of carrier lifetime in 4H-SiC epilayers by ion implantation," Appl. Phys. Lett. **90**(6), 472530 (2007).
[26]M. E. Bathen, A. Galeckas, J. Müting, H. M. Ayedh, U. Grossner, J. Coutinho, Y. K. Frodason, and L. Vines, "Electrical charge state identification and control for the silicon vacancy in 4H-SiC," npj Quantum Inf. **5**(1), 227 (2019).
[27]N. T. Son and I. G. Ivanov, "Charge state control of the silicon vacancy and divacancy in silicon carbide," J. Appl. Phys. **129**(21), 52131 (2021).
[28]S. Sasaki, K. Kawahara, G. Feng, G. Alfieri, and T. Kimoto, "Major deep levels with the same microstructures observed in n-type 4H-SiC and 6H-SiC," J. Appl. Phys. **109**(1), 528134 (2011).
[29]H. Nakane, M. Kato, Y. Ohkouchi, X. T. Trinh, I. G. Ivanov, T. Ohshima, and N. T. Son, "Deep levels related to the carbon antisite-vacancy pair in 4H-SiC," J. Appl. Phys. **130**(6), 59953 (2021).
[30]J. Zhang, J. Guo, Y. Zhang, Y. Cao, M. I. Dobynde, C. Li, Y. Yu, Y. Wang, S. Tang, Y. Qian, H. Zhao, Z. Sun, Y. Wang, and R. F. Wimmer-Schweingruber, "The 2022 February 15 solar energetic particle event at mars: A synergistic study combining multiple radiation detectors on the surface and in orbit of mars with models," Geophys. Res. Lett. **51**(19), 111775, https://doi.org/10.1029/2024GL111775 (2024).
[31]E. M. Klein, M. Sznajder, and P. Seefeldt, "Proton spectra for the interplanetary space derived from different environmental models," Front. Space Technol. **3**, 933340 (2022).
[32]A. N. Petrov, O. R. Grigoryan, and M. I. Panasyuk, "Energy spectrum of proton flux near geomagnetic equator at low altitudes," Adv. Space Res. **41**(8), 1269 (2008).
[33]Y. Tian, R. Li, J. Li, H. Li, X. Zheng, Z. Cheng, and J. Sun, "Effects of electric polarization and defect energy levels induced by ion irradiation on the electrical behavior of 4H-SiC Schottky barrier diodes," J. Phys. D:Appl. Phys. **56**, 355110 (2023).
[34]N. T. Son, X. T. Trinh, L. S. Løvlie, B. G. Svensson, K. Kawahara, J. Suda, T. Kimoto, T. Umeda, J. Isoya, T. Makino, T. Ohshima, and E. Janzén, "Negative-U system of carbon vacancy in 4H-SiC," Phys. Rev. Lett. **109**, 187603 (2012).
[35]I. Pintilie, L. Pintilie, K. Irmscher, and B. Thomas, "Formation of the $Z_{1/2}$ deep-level defects in 4H-SiC epitaxial layers: Evidence for nitrogen participation," Appl. Phys. Lett. **81**, 4841 (2002).
[36]X. Wang, H. Zhang, T. Baba, H. Jiang, C. Liu, Y. Guan, O. Elleuch, T. Kuech, D. Morgan, J.-C. Idrobo, P. M. Voyles, and I. Szlufarska, "Radiation-induced segregation in a ceramic," Nat. Mater. **19**(9), 992 (2020).
[37]M. Bockstedte, A. Mattausch, and O. Pankratov, "*Ab initio* study of the annealing of vacancies and interstitials in cubic SiC: Vacancy-interstitial recombination and aggregation of carbon interstitials," Phys. Rev. B **69**, 235202 (2004).
[38]W. J. Weber, W. Jiang, and S. Thevuthasan, "Defect annealing kinetics in irradiated 6H-SiC," Nucl. Instrum. Methods Phys. Res., Sect. B **166–167**, 410 (2000).
[39]J. M. Rafí, G. Pellegrini, P. Godignon, G. Rius, V. Dauderys, I. Tsunoda, M. Yoneoka, K. Takakura, G. Kramberger, and M. Moll, "Low-temperature annealing of electron, neutron, and proton irradiation effects on SiC radiation detectors," IEEE Trans. Nucl. Sci. **70**, 2285 (2023).
[40]P. Hazdra and J. Vobecký, "Radiation defects created in n-type 4H-SiC by electron irradiation in the energy range of 1–10 MeV," Phys Status Solidi A **216**, 17 (2019).
[41]J. Vobecký, P. Hazdra, S. Popelka, and R. K. Sharma, "Impact of electron irradiation on the ON-state characteristics of a 4H-SiC JBS diode," IEEE Trans. Electron Devices **62**, 6 (2015).
[42]T. Kimoto, K. Kawahara, B. Zippelius, E. Saito, and J. Suda, "Control of carbon vacancy in SiC toward ultrahigh-voltage power devices," Superlattices Microstruct. **99**, 151 (2016).

[43]R. Karsthof, M. E. Bathen, A. Galeckas, and L. Vines, "Conversion pathways of primary defects by annealing in proton-irradiated n-type 4H-SiC," Phys. Rev. B **102**(18), 184111 (2020).
[44]K. Szász, V. Ivády, I. A. Abrikosov, E. Janzén, M. Bockstedte, and A. Gali, "Spin and photophysics of carbon-antisite vacancy defect in 4H silicon carbide: A potential quantum bit," Phys. Rev. B **91**(12), 121201 (2015).
[45]Q. Liu, J. Deng, Y. Sun, Z. Wang, and S. Song, "Characteristics of interacting carbon-antisite-vacancies in 4H silicon carbide," AIP Adv. **13**, 12 (2023).
[46]F. C. Beyer, C. G. Hemmingsson, H. Pedersen, A. Henry, J. Isoya, N. Morishita, T. Ohshima, and E. Janzén, "Capacitance transient study of a bistable deep level in e^--irradiated n-type 4H-SiC," J. Phys. D:Appl. Phys. **45**(45), 455301 (2012).